Translational repression of pre-formed cytokine-encoding mRNA prevents chronic activation of memory T cells

Fiamma Salerno [1], Sander Engels [1], Maartje van den Biggelaar [2], Floris P. J. van Alphen [2], Aurelie Guislain [1], Wanqi Zhao [1], Deborah L. Hodge [3], Sarah E. Bell [4], Jan Paul Medema [5], Marieke von Lindern [1], Martin Turner [4], Howard A. Young [3], and Monika C. Wolkers [1,*]

[1]Sanquin Research, Department of Hematopoiesis, and Landsteiner Laboratory, Academic Medical Centre (AMC), University of Amsterdam, Amsterdam, The Netherlands [2]Sanquin Research, Department of Plasma Proteins, Amsterdam, The Netherlands [3]Laboratory of Experimental Immunology, Cancer and Inflammation Program, Center for Cancer Research, National Cancer Institute at Frederick, MD, USA [4]Laboratory of Lymphocyte Signalling and Development, The Babraham Institute, Babraham, UK [5]Laboratory of Experimental Oncology and Radiobiology (LEXOR), Center for Experimental Molecular Medicine (CEMM), Academic Medical Center (AMC), University of Amsterdam, Amsterdam, The Netherlands

Abstract

Memory T cells are critical for the immune response to recurring infections. Their instantaneous reactivity to pathogens is empowered by the persistent expression of cytokine-encoding mRNAs. How the translation of proteins from pre-formed cytokine-encoding mRNAs is prevented in the absence of infection has remained unclear. Here we found that protein production in memory T cells was blocked via a 3€ untranslated region (3€UTR)-mediated process. Germ-line deletion of AU-rich elements (AREs) in the *Ifng*-3€UTR led to chronic cytokine production in memory T cells. This aberrant protein production did not result from increased expression and/or half-life of

Keywords

post-transcriptional regulation; memory T cells; AU-rich elements; Interferon-γ (IFN-γ); cytokines; ZFP36L2/Tis11D; ARE-binding proteins; mRNA translation

Memory T cells (T_M cells) are critical for the immune response against recurring infections. Their longevity and tissue localization allows T_M cells to maintain effective immunity against bacteria, protozoa and viruses[1–3]. A key characteristic of both CD8+ and CD4+ T_M cells is their capacity to produce substantial amounts of effector molecules within a few hours upon re-infection[4–6]. This rapid responsiveness limits pathogen spreading and recruits innate immune cells to the site of infection[7,8]. The swift recall response by T_M cells is supported by changes in chromatin structure and epigenetic modifications that increase transcription rates of genes encoding effector molecules[9–11]. As a result, mRNAs encoding pro-inflammatory cytokines such as interferon gamma (IFN-γ) are increased in human and mouse T_M cells when compared to naive T cells[12–14]. Pre-formed *Ifng* and *Tnf* mRNA is critical for the instantaneous protein production upon T cell activation[15]. Such pre-formed mRNA is advantageous for recall responses, as cytokines can be rapidly produced without initiating transcription. However, chronic cytokine production can elicit severe immunopathology[16,17]. Because pre-formed mRNA is ready to be translated, it is critical that protein production is tightly regulated, and strictly confined to reactivated T_M cells. How chronic and undesired cytokine production from pre-formed mRNA is prevented in T_M cells is to date unknown.

Post-transcriptional regulation is a critical modulator of protein production by regulating mRNA stability, changing mRNA localization and inhibiting protein translation. RNA-binding proteins (RBPs) and non-coding RNAs, such as micro-RNAs, mediate these processes by binding to sequences located in the 3€ untranslated region (3€UTR) of the mRNA[18–20]. For instance, global down-regulation of micro-RNAs during T cell activation promotes the acquisition of effector functions[21,22]. Whereas micro-RNAs activity is primarily associated with keeping T cells quiescent, RBPs can directly promote T cell effector responses. The activity of RBPs can be regulated by different post-translational modifications[23,24]. RBPs bind to secondary RNA structures like the constitutive decay element (CDE)[25], or to short single-stranded sequences, such as GU-rich or AU-rich elements (AREs)[26]. The 3€UTR of many cytokines, including *Ifng, Tnf* and *Il2,* contain AREs that consist of one or several AUUUA pentamers[27]. RBP binding to AREs is thought to primarily modulate mRNA stability, which is supported by the observation that many ARE-bearing transcripts display a short mRNA half-life[28].

We show here that rapid mRNA turnover was not sufficient to avoid chronic protein production in T_M cells. Rather, AREs were critical to block translation of pre-formed mRNA, a process that was mediated by the ARE-binding protein ZFP36L2. Thus, T_M cells could contain deployment-ready mRNA for rapid recall responses because the recruitment of pre-formed cytokine mRNA to ribosomes was prevented in the absence of infection.

RESULTS

The 3€UTR of Ifng determines protein expression levels in T_M cells

We first examined if the *Ifng* 3€UTR regulated protein production in T_M cells. We fused the murine *Ifng* 3€UTR to a GFP reporter gene (hereafter *GFP-Ifng*3€UTR) under the control of the murine PGK-1 promoter. We retrovirally transduced OTI TCR transgenic T_M CD8$^+$ cells expressing the congenic marker CD45.1 with *GFP-Ifng*3€UTR, or with GFP that lacked a 3€UTR (hereafter $GFP_{control}$). The next day, 1000 sorted *GFP-Ifng*3€UTR OTI or $GFP_{control}$ OTI cells were transferred into naive C57BL/6J/CD45.2 recipient mice followed by infection with the intracellular bacterium *Listeria monocytogenes* genetically engineered to express ovalbumin (LM-OVA)[29] the next day. We found identical percentages of GFP-*Ifng*3€UTR and of $GFP_{control}$ OTI cells in the blood of recipient mice at all time points measured (Fig. 1a). The $GFP_{control}$ OTI cells expressed constant levels of GFP throughout the infection as determined by the GFP mean fluorescence intensity (GFP-MFI; Supplementary Fig. 1a). In contrast, the GFP-MFI in *GFP-Ifng*3€UTR OT-I cells increased at day 9 post infection, and dropped at day 13, when the infection was resolved (Supplementary Fig. 1a). At day 35 post infection, the GFP-MFI was about six-fold lower for GFP-*Ifng*3€UTR OTI cells than for $GFP_{control}$ OTI cells isolated from blood, liver and spleen (Fig. 1b,c and Supplementary Fig.1b). Reactivation of OTI cells isolated at day 35 post infection with the $OVA_{257-264}$ peptide did not alter the MFI of $GFP_{control}$ OTI cells ($p=0.4$), but increased the expression of *GFP-Ifng*3€UTR compared to non-activated cells ($p=0.01$, Fig. 1b,c).

Spleen-derived $GFP_{control}$ $CD4^+$ and $CD8^+$ T cells from C57BL/6J mice showed high GFP-MFI when cultured in IL-7 for several days in the absence of antigen (hereafter ‚resting€), and reactivation for 4h with PMA+ionomycin did not alter the GFP-MFI. In contrast, GFP-*Ifng*

GFP-MFI as $GFP_{control}$

precurser cells (MPEC) was indistinguishable between IFNγ-ARE-Del and wild-type OTI cells (Fig. 3b, Supplementary Fig. 3a).

Despite the normal differentiation into T

IFNG$_{\text{MUT1•5}}$ variant, *IFNG*$_{MUT1•5}$

CD44^{hi} T cells was comparable to that of IFNγ-ARE-DEL T cells (Fig. 5h; Supplementary Fig. 5g), indicating the ARE-independent degradation of *Ifng* mRNA did not require ZFP36L2. In addition, the amount of miR-29a/b, which can affect *Ifng* mRNA expression[39,40]

Supplementary Fig. 7a). 17 proteins were significantly less abundant in stimulated T cells, including CD62L (Sell, Fig. 7a), which is rapidly downregulated upon T cell activation. Conversely, 37 proteins were significantly induced in stimulated $CD44^{hi}$ OTI cells, including the early activation marker CD69 and the pro-inflammatory cytokines IFN-γ, TNF and IL-2 (Fig. 7a). Of note, 32 of these 37 proteins were generated from ARE-containing mRNAs (Fig. 7a; Supplementary Fig. 7a).

We next determined the mRNA levels of these rapidly induced proteins in T_M cells. 52 out of the 54 proteins that altered their expression profile upon activation of $CD44^{hi}$ OTI cells were annotated in T_{EM} and T_{CM} cells specific for the lymphochoriomeningitis virus (LCMV)[42]. The mRNAs for the 17 proteins that were enriched in the $CD44^{hi}$ OTI cells were also expressed in LCMV-specific T_{EM} and T_{CM} cells (Fig. 7b, Supplementary Fig. 7b). The mRNAs of the 35 proteins that were rapidly induced in $CD44^{hi}$ OTI cells greatly varied in expression in T_{EM} and T_{CM} cells (Fig. 7b, Supplementary Fig. 7b). LCMV-specific T_{EM} and T_{CM} cells expressed the mRNA for 29 of the 35 (82.9%) rapidly generated proteins (Fig. 7b, Supplementary Fig. 7b). For 22 of these 35 proteins (62.9%), the peptide abundance was below detection limit in non-activated $CD44^{hi}$ T cells (Supplementary Fig. 7a), indicating that these 22 mRNAs are putatively blocked from translation in T_M cells.

ZFP36L2 binds to ARE-containing mRNA with a tandem zinc finger[43] that requires two AREs for interaction. Of the 35 rapidly-induced proteins, 26 ARE-containing transcripts encompassed at least 2 AREs (defined as AUUUA) within the 3′UTR (Supplementary Table 1). We focused on 11 putative target genes that fulfilled the following criteria: they contained 2 AREs in most of their transcript variants (Supplementary Table 1), and they expressed pre-formed mRNA in T_M cells (Supplementary Fig. 7b). We measured ZFP36L2 binding to these endogenously expressed mRNAs using native RNA-immunoprecipitation in resting OTI cells. Of the 11 tested mRNAs, 6 mRNAs were significantly enriched in resting T cells compared to the IgG control pull down: *Ifng, Tnf, Irf4, Junb, Zfp36l1* and *Pim1* (Fig. 7c), indicating that ZFP36L2 targets several ARE-containing pre-formed mRNAs in T_M cells.

ZFP36L2 rapidly releases pre-formed mRNA upon activation

Because pre-formed mRNA drives rapid cytokine production upon T cell activation[15], we tested if T cell activation supports the release of pre-formed mRNA from ZFP36L2. As determined by RNA-immunoprecipitation, ZFP36L2 binding to *Ifng* mRNA was significantly reduced in OTI cells reactivated with $OVA_{257-264}$ for 2h compared to non-activated resting OTI cells (Fig. 7d). Of note, loss of mRNA binding upon reactivation coincided with rapid downregulation of *Zfp36l2* mRNA, but ZFP36L2 protein remained unaltered (Supplementary Fig. 7d). ZFP36L2 also rapidly dissociated from *Tnf* and *Pim1* mRNA upon T cell activation, while its binding to *Irf4, Junb* and *Zfp36l1* mRNA did not change compared to non-activated T cells (Fig. 7d). Peptides for IFN-γ, TNF and Pim1 were below detection limit in non-activated $CD44^{hi}$ T cells in the proteomics analysis (Supplementary Fig. 7a), further pointing to a block of mRNA translation. *Tnf* mRNA was significantly enriched in the ribosome-enriched fraction of $Zfp36l2^{cKO}$ $CD8^+$ and $CD4^+$ $CD44^{hi}$ T cells compared to wild-type T cells (Fig. 7e), and TNF production was found in $CD8^+$ and $CD4^+$ $CD44^{hi}$ T cells in the absence of stimulation (Fig. 7f). These observations

recombinant murine Interleukin 7 (rmIL-7, 1ng/ml, PeproTech), or with plate-bound anti-CD3 (2…g/ml, eBioscience) and soluble anti-CD28 (1…g/ml, Bioceros) antibodies. Cells were harvested and retrovirally transduced as described. T cells were maintained with 10ng/ml rmIL-7 and reactivated with 100nM or 1…M OVA

RNA immunoprecipitation and Western Blot

Cytoplasmic lysates of resting WT or IFN-γ-ARE-Del OTI T cells (250†10^6 cells per condition) were prepared using lysis buffer (10mM HEPES pH 7.0, 100mM KCl, 5mM $MgCl_2$, 0.5% NP40) freshly supplemented with 1mM DTT, 40U/ml RNase OUT (both Invitrogen), 0.4mM vanadylribonucleoside complex RNase inhibitor (NEB) and 1% EDTA-free protease/phosphatase inhibitor cocktail (Thermo Scientific). Protein G dynabeads (Thermo Scientific) were prepared as previously described[60]. The lysate was immunoprecipitated for 2h at 4„C with a rabbit anti-ZFP36L2 polyclonal antibody (ab70775) or a rabbit polyclonal IgG isotype control (ab27478, both Abcam). RNA was extracted directly from beads by using Trizol, and mRNA expression was measured by RT-PCR as described above. Specificity of the RNA-IP assay was tested by western blot using a rat pan-ZFP36 antibody generated in the laboratory of M. Turner (unpublished data). This antibody is directed against the C terminus of ZFP36L1 and recognizes all three ZFP36 family members.

1†10^6 FACS-sorted CD8$^+$CD44^{low} and CD8CD44^{hi} T cells were lysed according to standard procedures. Proteins were separated on a 10% SDS-PAGE gel and transferred onto

30…g *in vitro* transcribed RNA and 10mg protein were used. RNA-bound proteins were eluted by adding 1…g RNaseA (Thermo Scientific) and 100…l 100mM Tris-Hcl pH 7.5 (Gibco-Invitrogen). Proteins were reduced, alkylated and digested into peptides using trypsin. Peptides were desalted and concentrated using Empore-C18 StageTips[61] eluted with 0.5% (v/v) acetic acid, 80 % (v/v) acetonitrile. Sample volume was reduced by SpeedVac and supplemented with 2% acetonitrile, 0.1% TFA.

Proteomic analysis of OTI memory T cells

Triplicates of 2†10^6 FACS-sorted CD8$^+$CD44^{hi} OTI T cells were incubated for 2h in IMDM containing 5% FCS and 1…g/ml BrfA with or without the presence of 100nM $OVA_{257•264}$ peptide. Cells were washed twice with ice-cold PBS and cell pellets were snap frozen in liquid nitrogen. Cells were lysed in 40…l 1% Sodium Deoxy Cholate, 40mM Chloro Acetamide (both Sigma Aldrich), 10mM TCEP (Thermo Scientific), and 100mM Tris-Hcl pH 8 (Life Technologies), boiled at 95„ for 5 minutes and sonicated for 10 minutes in a Sonifier bath (Branson). An equal volume of 50mM ammonium bicarbonate (Sigma Aldrich) was added, containing 600ng Trypsin Gold (Promega). Samples were digested overnight at room temperature, acidified by addition of 1…l trifluoroacetic acid (Thermo Scientific) and loaded on in-house prepared SDB-RPS StageTips (Empore). Peptides were desalted and eluted in three fractions by increasing concentrations of ammonium formate (100mM and 150mM) or 5% (v/v) ammonium hydroxide and acetonitrile (40%, 60% and 80% v/v)[62]. Sample volume was reduced by SpeedVac and supplemented with 2% acetonitrile, 0.1% TFA.

Mass spectrometry data acquisition

Tryptic peptides were separated by nanoscale C18 reverse chromatography coupled on line to an Orbitrap Fusion Tribrid mass spectrometer via a NanoElectroSpray Ion Source (both Thermo Scientific). Peptides were loaded on a 20 cm 75•360…m inner-outer diameter fused silica emitter (New Objective) packed in-house with ReproSil-Pur C18-AQ, 1.9…m resin (Dr Maisch GmbH). The column was installed on a Dionex Ultimate3000 RSLC nanoSystem (Thermo Scientific) using a MicroTee union formatted for 360…m outer diameter columns (IDEX) and a liquid junction. The spray voltage was set to 2.15 kV. Buffer A was composed of 0.5% acetic acid and buffer B of 0.5% acetic acid, 80% acetonitrile. Peptides were loaded for 17 min at 300nl/min at 5% buffer B, equilibrated for 5 minutes at 5% buffer B (17•22min) and eluted by increasing buffer B from 5•15% (22•87min) and 15•38% (87•147min), followed by a 10 minute wash to 90% and a 5min regeneration to 5%. Survey scans of peptide precursors from 400 to 1500 m/z were performed at 120K resolution (at 200 m/z) with a 1.5†10^5 ion count target. Tandem mass spectrometry was performed by isolation with the quadrupole with isolation window 1.6, HCD fragmentation with normalized collision energy of 30, and rapid scan mass spectrometry analysis in the ion trap. The MS2 ion count target was set to 104 and the max injection time was 35ms. Only those precursors with charge state 2•7 were sampled for MS2. The dynamic exclusion duration was set to 60s with a 10ppm tolerance around the selected precursor and its isotopes. Monoisotopic precursor selection was turned on. The instrument was run in top speed mode with 3s cycles. All data were acquired with Xcalibur software.

Mass spectrometry data analysis

The RAW mass spectrometry files were processed with the MaxQuant computational platform, 1.5.0.25 (RNA pull down) or 1.6.0.13 (memory OTI T cells)[63]. Proteins and peptides were identified using the Andromeda search engine by querying the human Uniprot database (downloaded February 2015, 89796 entries) for the RNA pull down, or the mouse Uniprot database (downloaded August 18, 2017, 51434 entries) for analysis of memory OTI T cells. Standard settings with the additional options match between runs, Label Free Quantification (LFQ), and unique peptides for quantification were selected. The generated ‚proteingroups.txt€ table was filtered for potential contaminants and reverse hits using Perseus 1.5.0.31 (RNA pull down) or 1.5.1.6 (memory OTI T cells). The LFQ values were transformed in log2 scale, the triplicates per experimental condition grouped, and proteins were filtered for at least three valid values in one of the experimental groups. Missing values were imputed by normal distribution (width=0.3, shift=1.8), assuming these proteins were close to the detection limit. To identify the proteins with the most prominent differences, we performed a two-sided *t*-test using an FDR of 5% and S0 of 0.4 (Volcano plot). Mass spectrometry data of resting and activated memory T cells (Fig. 7 and Supplementary Fig. 7) are deposited at PRIDE: PXD008051.

mRNA expression analysis and ARE determination

mRNA expression of LCMV-specific spleen-derived central memory (CM) and effector memory (EM) T cells was extracted from Mackay *et al.*[42] (GEO accession number: GSE70813). Reads per million mapped reads (RPM) were transformed as log2-normalized counts using DESeq2[64].

To determine the presence of ARE sequences in mRNAs, the 3€UTR sequences of all murine transcripts were downloaded from Ensembl BioMart (release May 2015) and compared to transcripts present in the RNAseq data set of memory T cells[42]. AREs (sequence motif ATTTA) were counted in all 3€UTR variants. When multiple transcripts were present for a gene, we used the minimum, maximum, and average count of AREs. Resulting data were combined with gene expession data by gene symbols.

Statistical analysis

Statistical analysis between groups was performed with GraphPad Prism 6, using the 2-tailed Student *t* test when comparing 2 groups, or one-way ANOVA test with Dunnett correction when comparing > 2 groups. *P* values <0.05 were considered statistically significant.

Supplementary Material

Refer to Web version on PubMed Central for supplementary material.

ACKNOWLEDGEMENTS

advice, and D. Amsen, M. Nolte, and R. van Lier for critical reading of the manuscript. M.T. and S.E.B. are supported by the Biotechnology and Biological Sciences Research Council. D.H. and H.A.Y. are funded through the intramural research program of the U.S. NCI/NIH. The use of materials and reagents does not imply any endorsement of these products by the U.S. government. This research was supported by the Dutch Science Foundation (VENI grant 916.76.127/VIDI grant 917.14.314, to M.C.W.).

REFERENCES

1. Masopust D & Schenkel JM The integration of T cell migration, differentiation and function. Nature reviews 13, 309•320 (2013).
2. Sheridan BS & Lefrancois L Regional and mucosal memory T cells. Nat Immunol 12, 485•491 (2011). [PubMed: 21739671]
3. Harty JT, Tvinnereim AR & White DW CD8+ T cell effector mechanisms in resistance to infection. Annu Rev Immunol 18, 275•308 (2000). [PubMed: 10837060]
4. Veiga-Fernandes H, Walter U, Bourgeois C, McLean A & Rocha B Response of naive and memory CD8+ T cells to antigen stimulation in vivo. Nat Immunol 1, 47•53 (2000). [PubMed: 10881174]
5. London CA, Lodge MP & Abbas AK Functional responses and costimulator dependence of memory CD4+ T cells. J Immunol 164, 265•272 (2000). [PubMed: 10605020]
6. Whitmire JK, Eam B & Whitton JL Tentative T cells: memory cells are quick to respond, but slow to divide. PLoS Pathog 4, e1000041 (2008).
7. Guidotti LG & Chisari FV Noncytolytic control of viral infections by the innate and adaptive immune response. Annu Rev Immunol 19, 65•91 (2001). [PubMed: 11244031]
8. Soudja SM, Ruiz AL, Marie JC & Lauvau G Inflammatory monocytes activate memory CD8(+) T and innate NK lymphocytes independent of cognate antigen during microbial pathogen invasion. Immunity 37, 549•562 (2012). [PubMed: 22940097]
9. Weng NP, Araki Y & Subedi K The molecular basis of the memory T cell response: differential gene expression and its epigenetic regulation. Nature reviews 12, 306•315 (2012).
10. Wherry EJ et al. Molecular signature of CD8+ T cell exhaustion during chronic viral infection. Immunity 27, 670•684 (2007). [PubMed: 17950003]
11. Philip M et al. Chromatin states define tumour-specific T cell dysfunction and reprogramming. Nature 545, 452•456 (2017). [PubMed: 28514453]
12. Kaech SM, Hemby S, Kersh E & Ahmed R Molecular and functional profiling of memory CD8 T cell differentiation. Cell 111, 837•851 (2002). [PubMed: 12526810]
13. Swanson BJ, Murakami M, Mitchell TC, Kappler J & Marrack P RANTES production by memory phenotype T cells is controlled by a posttranscriptional, TCR-dependent process. Immunity 17, 605•615 (2002). [PubMed: 12433367]
14. Willinger T, Freeman T, Hasegawa H, McMichael AJ & Callan MF Molecular signatures distinguish human central memory from effector memory CD8 T cell subsets. J Immunol 175, 5895•5903 (2005). [PubMed: 16237082]
15. Salerno F, Paolini NA, Stark R, von Lindern M & Wolkers MC Distinct PKC-mediated

21. Bronevetsky Y et al. T cell activation induces proteasomal degradation of Argonaute and rapid remodeling of the microRNA repertoire. The Journal of experimental medicine 210, 417•432 (2013). [PubMed: 23382546]
22. Wu H et al. miRNA profiling of naive, effector and memory CD8 T cells. PloS one 2, e1020 (2007).
23. Garneau NL, Wilusz J & Wilusz CJ The highways and byways of mRNA decay. Nat Rev Mol Cell Biol 8, 113•126 (2007). [PubMed: 17245413]
24. Grammatikakis I, Abdelmohsen K & Gorospe M Posttranslational control of HuR function. Wiley Interdiscip Rev RNA (2016).
25. Jeltsch KM et al. Cleavage of roquin and regnase-1 by the paracaspase MALT1 releases their cooperatively repressed targets to promote T(H)17 differentiation. Nat Immunol 15, 1079•1089 (2014). [PubMed: 25282160]
26. Vlasova-St Louis I & Bohjanen PR Post-transcriptional regulation of cytokine signaling by AU-rich and GU-rich elements. J Interferon Cytokine Res 34, 233•241 (2014). [PubMed: 24697201]
27. Beisang D & Bohjanen PR Perspectives on the ARE as it turns 25 years old. Wiley Interdiscip Rev

62. Kulak NA, Pichler G, Paron I, Nagaraj N & Mann M Minimal, encapsulated proteomic-sample processing applied to copy-number estimation in eukaryotic cells. Nat Methods 11, 319•324 (2014). [PubMed: 24487582]
63. Cox J & Mann M MaxQuant enables high peptide identification rates, individualized p.p.b.-range mass accuracies and proteome-wide protein quantification. Nat Biotechnol 26, 1367•1372 (2008). [PubMed: 19029910]
64. Love MI, Huber W & Anders S Moderated estimation of fold change and dispersion for RNA-seq data with DESeq2. Genome Biol 15, 550 (2014). [PubMed: 25516281]
65. Di Tommaso P et al. T-Coffee: a web server for the multiple sequence alignment of protein and RNA sequences using structural information and homology extension. Nucleic acids research 39, W13•17 (2011). [PubMed: 21558174]

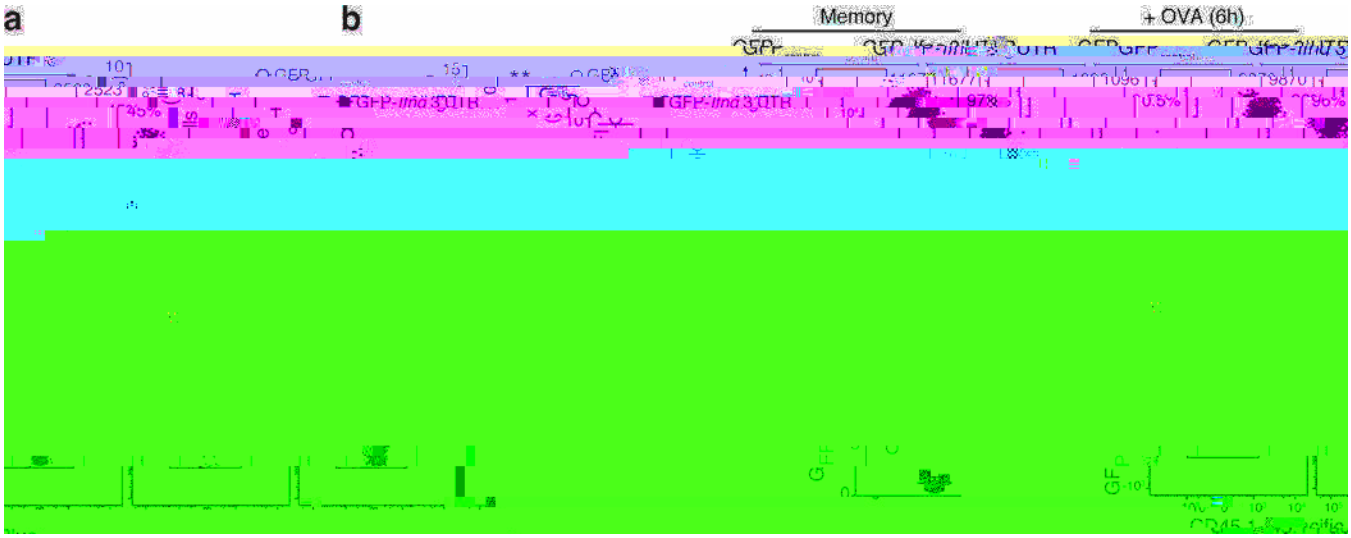

Figure 1: The 3€UTR of *Ifng* governs GFP expression in memory T cells *in vivo*

(a) Blood samples of LM-OVA infected C57BL/6J/CD45.2 recipient mice were analyzed for the presence of CD45.1$^+$ OTI cells expressing GFP-*Ifng* 3€UTR or GFP$_{control}$ reporter (n=10/group). GFP-MFI levels measured directly *ex vivo* in (b) spleen- and in (c) liver-residing OTI cells 35 days after infection. [Unpaired Student *t* test; n=5 mice per group; **p<0.005]. Representative GFP expression in memory OTI cells directly *ex vivo* (memory), and upon reactivation with OVA$_{257-264}$ peptide (+ OVA (6h)). Numbers in plots depict the GFP-MFI of the total population (top number) and the percentage of T cells within the upper gate that express high GFP levels (bottom number). Data shown are representative of 2

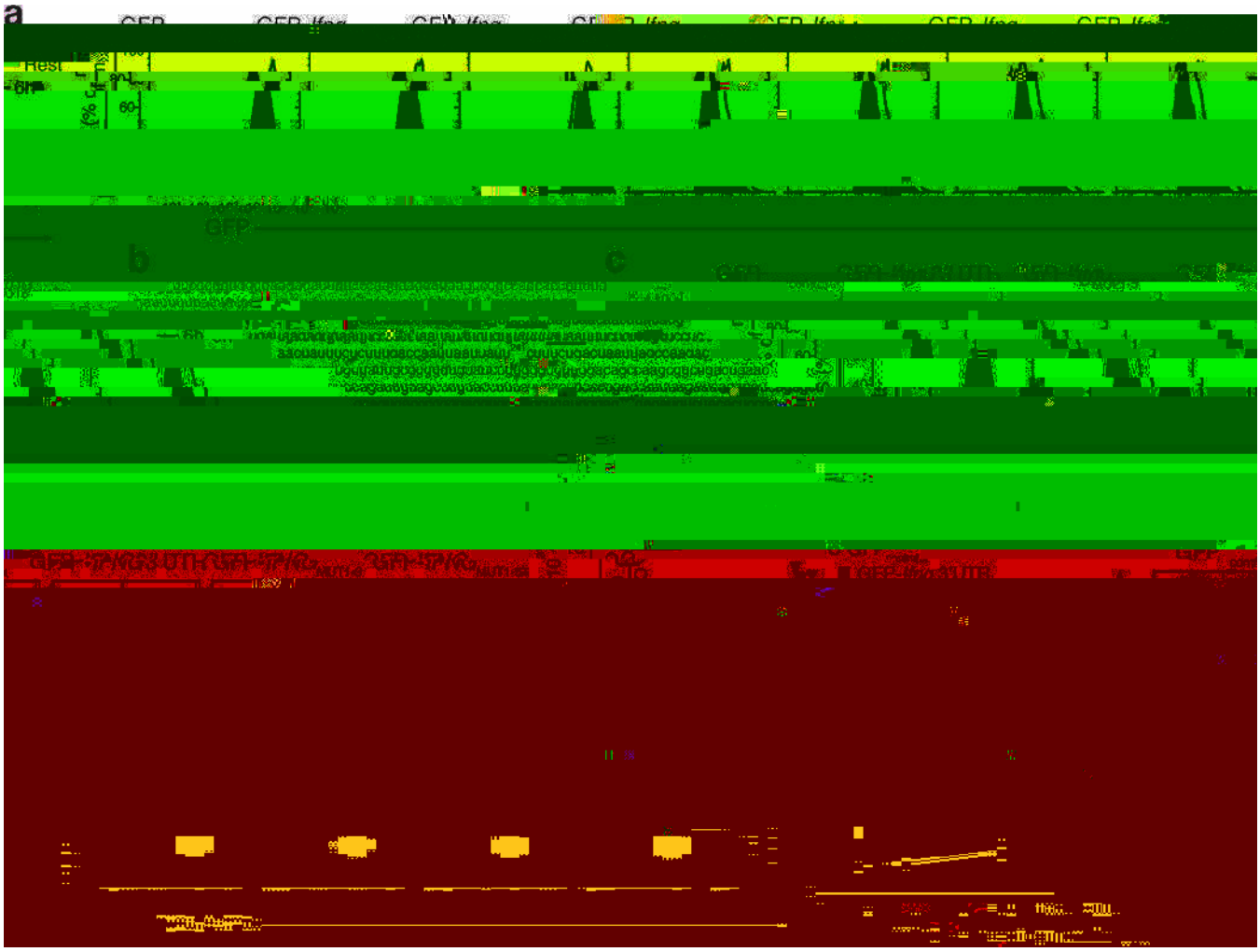

Figure 2: AU-rich elements within the Ifng 3€UTR determine protein production in mouse and human T cells

OTI cells were transduced with deletion mutants (a) or with ARE mutants of the full length murine *Ifng* 3€UTR (c-e). (b) Sequence of the murine *Ifng* 3€UTR. AREs are underlined. (a,c) Representative GFP levels of resting OTI cells (gray histograms), and after reactivation with $OVA_{257•264}$ peptide for 6h (black lines). (d) GFP-MFI of resting OTI cells transduced with indicated ARE mutants. (e) Fold increase of GFP-MFI upon activation with $OVA_{257•264}$ peptide compared to non-activated GFP-expressing T cells. Data are presented as mean‡SD of at least 3 independently performed experiments [one-way ANOVA with Dunnett€s multiple comparison to the control vector; n=8 mice per group; *p<0.005; **p<0.0005]. (f) Human T cells were transduced with full length human GFP-*IFNG* 3€UTR (WT), or with ARE mutants. Dot plots depicting GFP-MFI levels from resting T cells (top), or from PMA/ionomycin reactivated T cells (bottom), with $CD8^+$ cells shown in black and $CD4^+$ T cells in gray. Data shown are representative of 4 individuals, and of 3 independently performed experiments. Compiled data are depicted in Supplementary Fig. 2d.

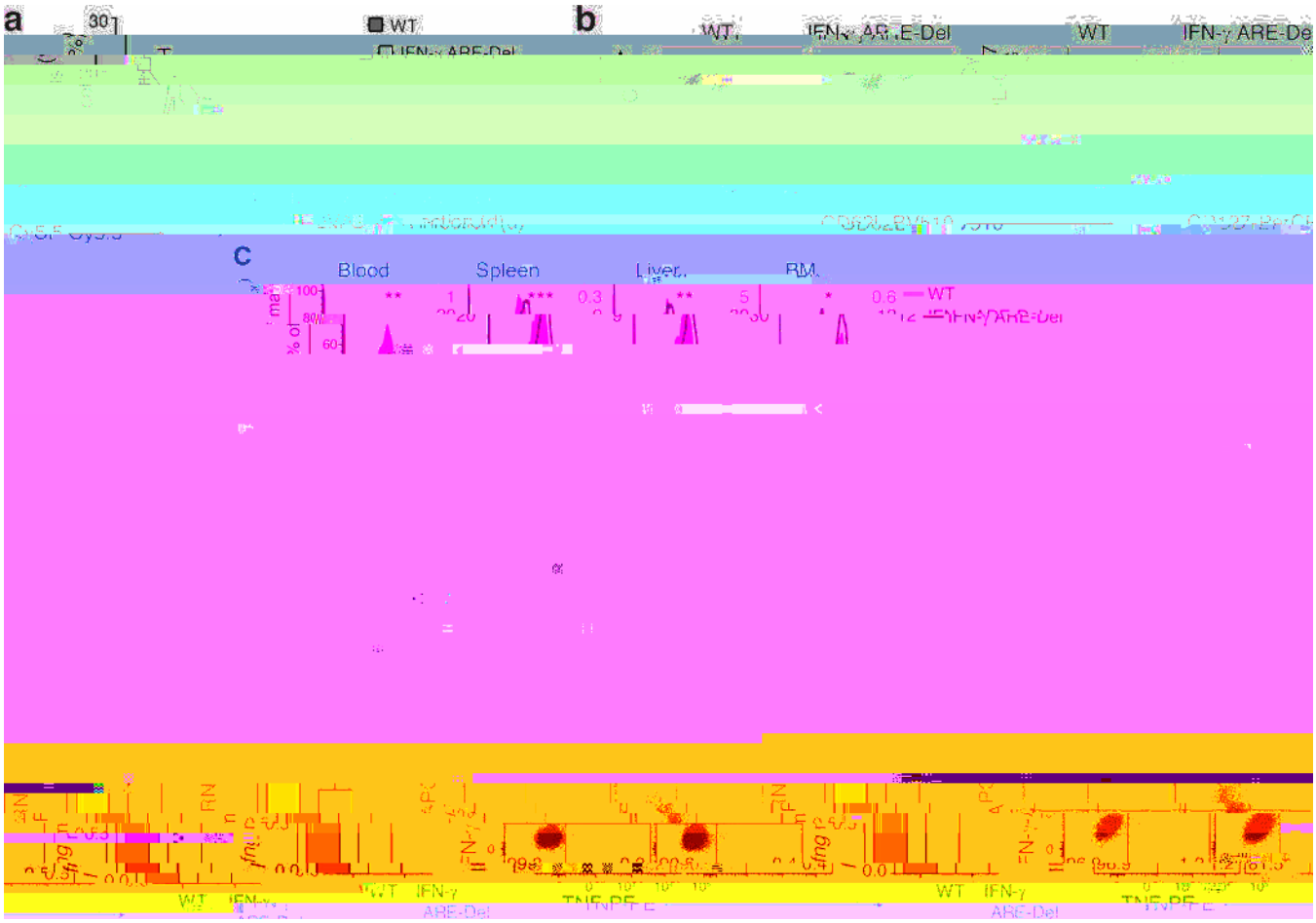

Figure 3: Deletion of AREs in the *Ifng* 3′UTR dysregulates protein production in T_M cells

(a) Percentage of CD8$^+$ OTI cells in blood drawn from LM-OVA infected mice at indicated time points (n=8 mice/group). (b) Representative dot plots of CD44/CD62L expression (left) and of CD127/KLRG1 expression (right) of wild-type OT-I/CD45.1 and IFN-γ-ARE-Del OT-I/CD45.2 cells 35 days post LM-OVA infection. Numbers in dot plots indicate percentage of OTI cells in corresponding gates. Compiled data are depicted in Supplementary Fig. 3a–c. (c) IFN-γ and TNF production measured in blood, spleen, liver, and bone marrow (BM)-derived T_M cells after 3h incubation with 1 μg/ml BFA. Histograms represent wild-type OT-I/CD45.1 (gray histograms) and IFN-γ-ARE-Del OT-I/CD45.2 (black lines) T_M cells. Numbers depict percentage of IFN-γ and TNF-producing T cells. IFN-γ and TNF MFI of wild-type and IFN-γ–ARE-Del T cells was compared with an Unpaired Student *t* test [n=4 mice/group; *p<0.05; **p<0.005; ***p<0.0005]. (d) Percentage of IFN-γ-producing T cells from spleen-residing wild-type (gray square) and IFN-γ-ARE-Del (white square) CD44^{hi}CD62L^{lo}CD 127^{lo} T_{EFF}, CD44^{hi}CD62L^{lo}CD127^{hi} T_{EM}, CD44^{hi}CD62L^{hi}CD127^{hi} T_{CM}, KLRG1^{hi}CD127^{lo} SLEC and KLRG1^{lo}CD127^{hi} MPEC cells 35 days post LM-OVA infection. [Unpaired Student *t* test; n=4 mice/group; **p<0.005; ***p<0.0005]. (e) *Ifng* mRNA expression in sorted splenic wild-type or IFN-γ-ARE-Del OT-I T_M cells 35 days post LM-OVA infection (pooled from 4 mice). Pooled data from 2 independently performed experiments. (f–g) IFN-γ protein (left) and mRNA levels

(right) of sorted spleen (f) and liver (g)-derived CD44^{hi}CD8^{+} wild-type and IFNγ-ARE-Del OT-I cells. Representative dot plots of 4 mice. mRNA data are pooled from 4 independently performed experiments (e-g) [Unpaired Student *t*-test; ns=not significant].

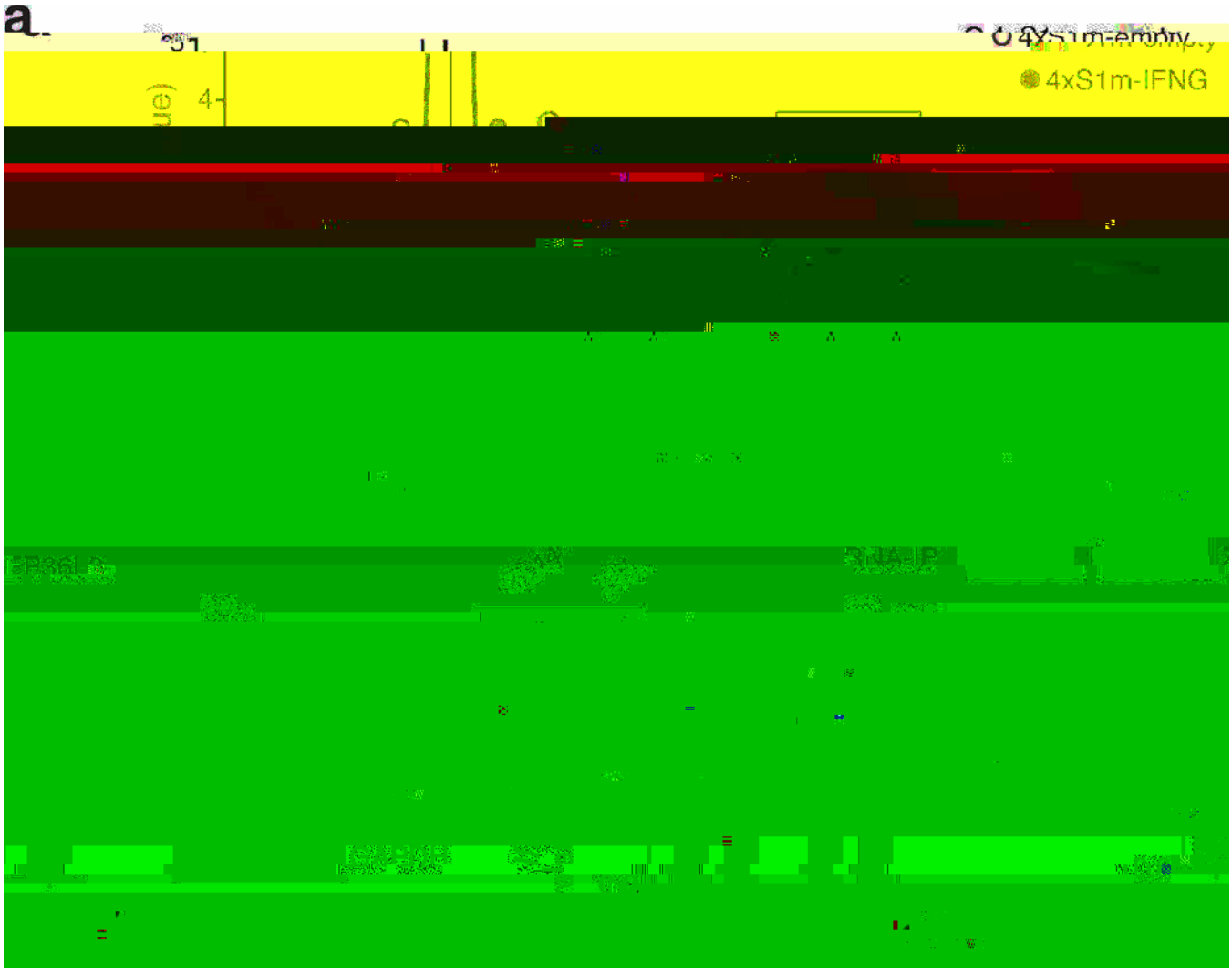

Figure 4: The RNA-binding protein ZFP36L2 binds Ifng mRNA

(a) Volcano plot of RBPs quantified by mass spectrometry from human resting T cell lysates pulled down with *in vitro* transcribed 4xS1m mRNA containing the 189nt long ARE-region of the human *IFNG* 3€UTR (4xS1m-*IFNG*), and the empty 4xS1m mRNA control (4xS1m-empty). Only proteins identified in all three replicates were considered putative ARE binders. Gray dots represent proteins that were significantly enriched in the presence of the *IFNG* 3€UTR, white dots represent proteins enriched in 4xS1m-empty [Two-sided *t*-test, FDR=0.05, S0=0.4)]. Heat map depicts Z-scored log2 LFQ values of ZFP36L1 and ZFP36L2 in all three replicates. (b-c) mRNA (b) and protein (c) expression of ZFP36L1 and ZFP36L2 in $CD44^{hi}CD8^{+}$ T cells. For the Western Blot, erythroblasts (EBL) were used as positive control[54]. (d) Binding of ZFP36L2 to *Ifng* mRNA in resting wild-type and IFN-γ-ARE-Del OTI cells was analyzed by RNA-immunoprecipitation. IgG isotype was used as control. Top: ZFP36L2 protein expression upon RNA-IP, detected with a pan anti-ZFP36 antibody at ‡55KD (specific size of ZFP36L2). Bottom: Data are pooled from 3 independently performed experiments (mean‡SD) [Unpaired Student *t*-test, n=4 mice/group; ns=not significant; *p<0.05].

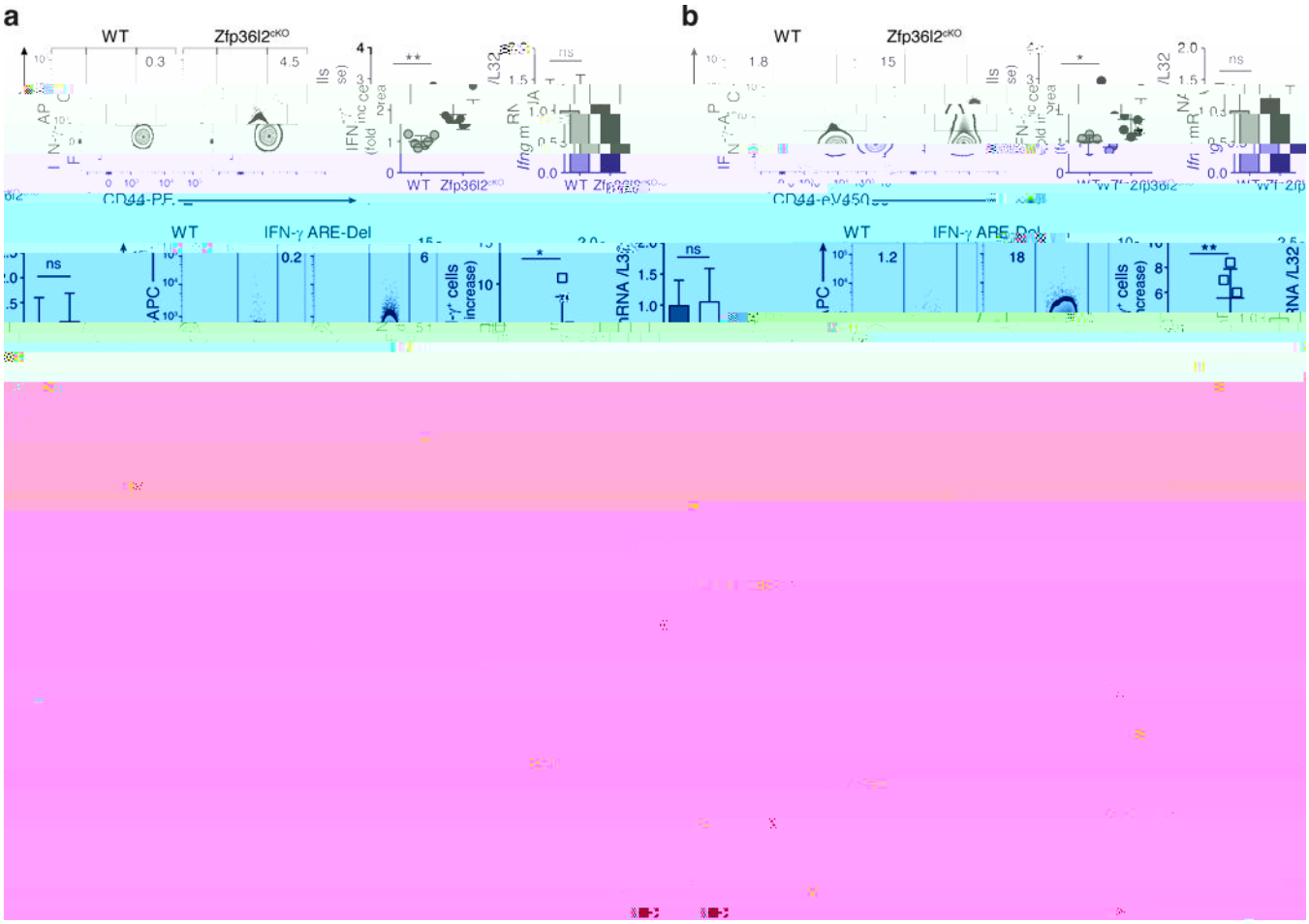

Figure 5: The ARE-binding protein ZFP36L2 represses IFNγ production in T_M cells
(a-b) IFN-γ

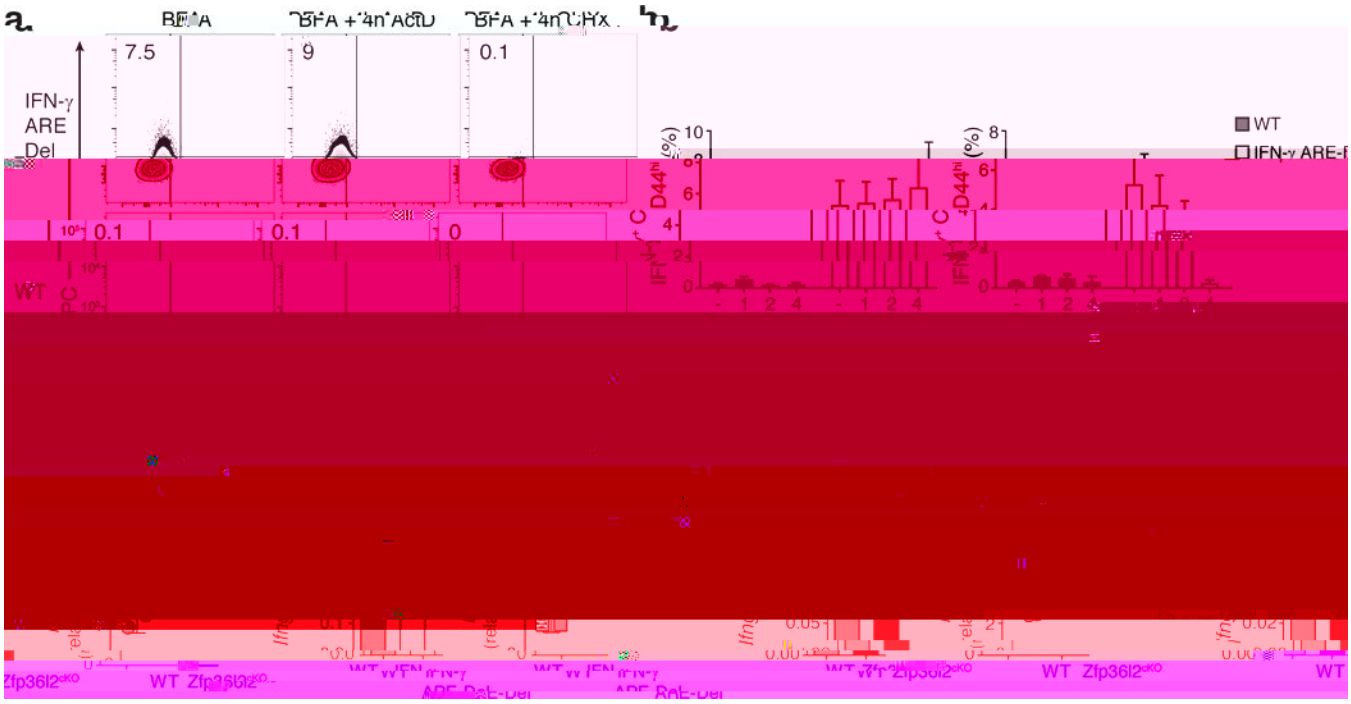

Figure 6: The interaction between AREs and ZFP36L2 blocks ribosome recruitment of pre-formed Ifng mRNA

(a) Representative IFN-γ and TNF production of sorted CD44^{hi}CD8^{+} memory-like IFN-γ-ARE-Del (upper panel) and wild-type (lower panel) OTI cells after 4h incubation with BFA alone (left), or with 1…g/ml ActD (middle) or 10…g/ml CHX (right). (b) Graphs depict percentage (mean‡SD of 4 independently performed experiments) of IFN-γ producing CD44^{hi}CD8^{+} wild-type or IFN-γ-ARE-Del OTI cells incubated with or without ActD (left) or CHX (right) for the entire culture of 4h, or for the last 2 or 1 h. (c-e) *Ifng* mRNA levels of cytosolic fractions from (c) CD44^{hi}CD8^{+} wild-type or IFN-γ-ARE-Del OTI cells, (d) CD44^{hi}CD8^{+} T cells or (e) CD44^{hi}CD4^{+} T cells from Zfp36l2^{cKO} or wild-type littermates. Left: mRNA input prior to fractionation; right: mRNA measured in the ribosome-enriched fraction after centrifugation of a sucrose cushion. Ribosome binding was determined by correlating the mRNA levels from untreated cytosolic fractions with that of EDTA-treated fractions. Results (mean‡SD) are pooled from (c; n=3•6 mice) and 2 (d-e; n=3 mice) independently performed experiments. [Unpaired Student *t* test; ns=not significant; *p<0.05].

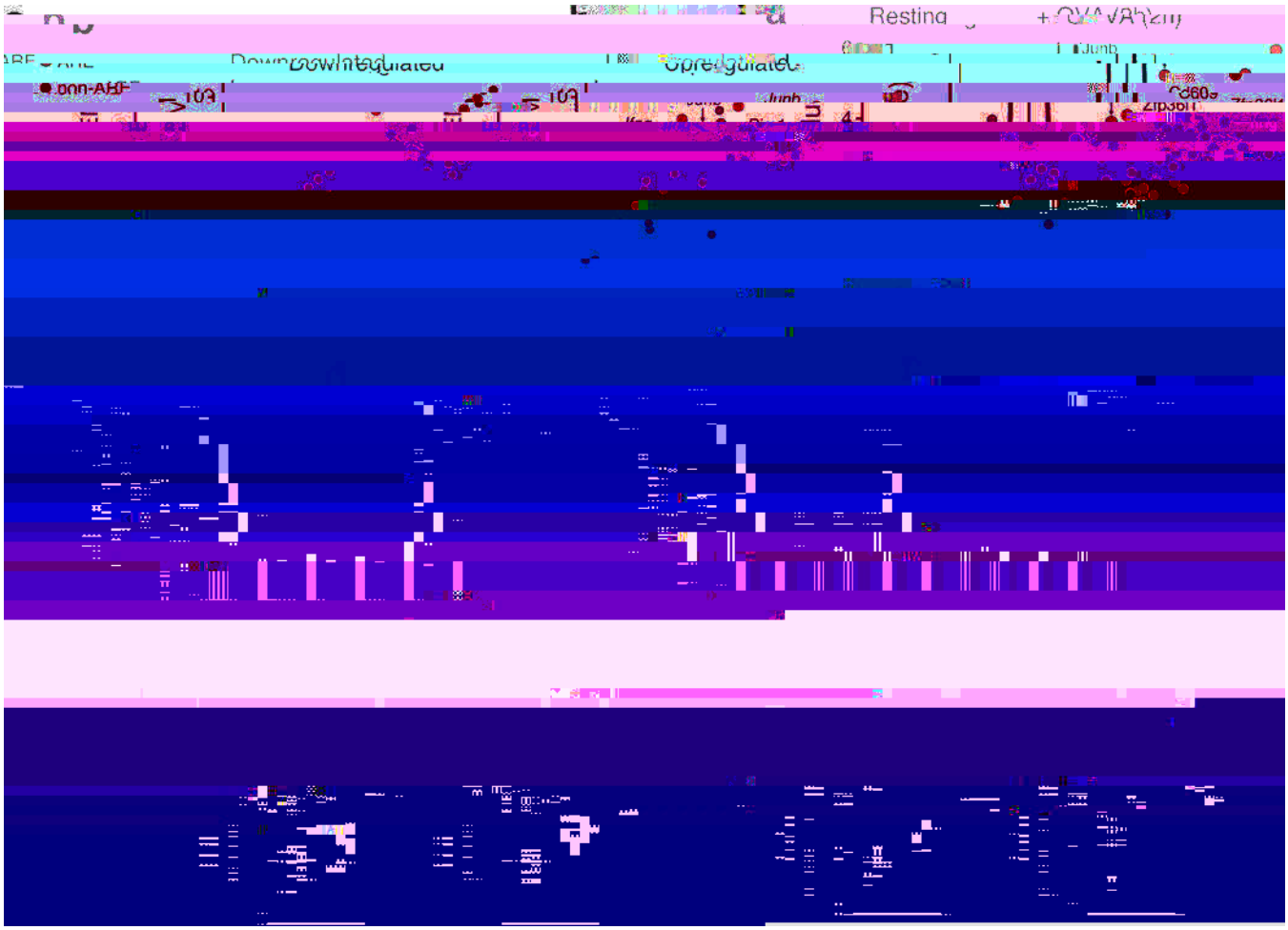

Figure 7: ZFP36L2 blocks translation of pre-formed mRNA from rapidly generated effector molecules

(a) Volcano plot of proteins quantified by mass spectrometry from splenic $CD44^{hi}CD8^{+}$ OTI cells that were cultured for 2h with or without 100nM of $OVA_{257-264}$ peptide in the presence of 1…g/ml BFA [n=3; Two-sided *t*-test; FDR=0.05, S0=0.4)]. (b) mRNA expression of LCMV-specific spleen-derived T_{EM} and T_{CM} cells from ref.[53]. Graphs display log2-normalized counts of reads per million mapped reads (RPM), of which a protein expression was significantly downregulated (left), or upregulated (right) upon T cell activation. (a-b) Red dots depict proteins that are encoded by ARE-containing transcripts. (c-d) ZFP36L2 RNA-immunoprecipitation of resting OTI cells compared to anti-IgG control RNA-IP (c) or compared to RNA-IP from cells reactivated for 2h with 100nM of $OVA_{257-264}$ peptide (values from anti-IgG control RNA-IP was substracted from each value) (d). Data are presented as mean±SD of 3–4 mice and pooled from 3 independently performed experiments. (e-f) $CD44^{hi}CD8^{+}$ and $CD4^{+}$ T cells were sorted from Zfp36l2 ^{cKO} or wild-type littermates. (e) Ribosome-bound *Tnf* mRNA was measured by RT-PCR following centrifugation through a sucrose cushion. Graphs display mRNA expression levels relative to paired EDTA-treated control samples (n=3). (f) Spontaneous TNF protein production was depicted as fold increase compared to wild-type mice (n=6). Results are

pooled from 2 independently performed experiments) [Unpaired Student *t* test; *p<0.05; ***p<0.0005].